Article

Scanning Kelvin Probe Imaging of the Potential Profiles in Fixed and Dynamic Planar LECs

Liam S. C. Pingree, Deanna B. Rodovsky, David C. Coffey, Glenn P. Bartholomew, and David S. Ginger

J. Am. Chem. Soc., **2007**, 129 (51), 15903-15910 • DOI: 10.1021/ja074760m

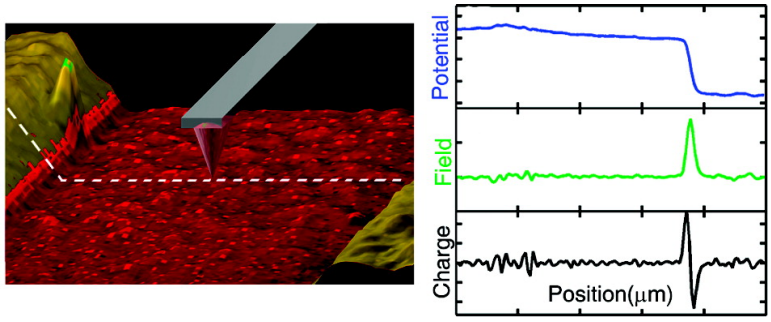

J|A|C|S
ARTICLES
Published on Web 12/04/2007

Scanning Kelvin Probe Imaging of the Potential Profiles in Fixed and Dynamic Planar LECs

Liam S. C. Pingree, Deanna B. Rodovsky, David C. Coffey, Glenn P. Bartholomew, and David S. Ginger*

Department of Chemistry, University of Washington, Box 351700, Seattle, Washington 98195-1700

Received June 28, 2007; E-mail: ginger@chem.washington.edu

Abstract: We measure the potential profiles of both dynamic and fixed junction planar light-emitting electrochemical cells (LECs) using Scanning Kelvin Probe Microscopy (SKPM) and compare the results against models of LEC operation. We find that, in conventional dynamic junction LECs formed using lithium trifluoromethanesulfonate (LiTf), poly(ethylene oxide) (PEO), and the soluble alkoxy-PPV derivative poly-[2-methoxy-5-(3′,7′-dimethyl-octyloxy)-*p*-phenylenevinylene (MDMO-PPV), the majority (>90%) of the potential is dropped near the cathode with little potential drop across either the film or the anode/polymer interface. In contrast, when examining fixed junction LECs where the LiTf is replaced with [2-(methacryloyloxy)ethyl] trimethylammonium 2-(methacryloyloxy)ethane-sulfonate (METMA/MES), the potential is dropped at both contacts during the initial poling. The potential profile evolves over a period of ~60 min under bias to achieve a final profile similar to that obtained in the LiTf systems. In addition to elucidating the differences between conventional dynamic LECs and fixed LECs incorporating cross-linkable ion pair monomers, the results on both systems provide direct evidence for a primarily "p-type" LEC consistent with the emitting junction near the cathode and relatively small electric fields across the bulk of the device for these two material systems.

1. Introduction

Recently, there has been renewed interest in light-emitting electrochemical cells (LECs) as advances have improved upon their transient response, efficiencies, and lifetimes.[1−6] Early formulations of LECs employed a light-emitting polymer, a salt, and a solid-state ionic transport agent to allow for the formation of a solid-state electrochemiluminescent device.[7] The ions in this device are relatively mobile, and the dynamic redistribution of ions under an applied bias lowers the barrier to charge injection into the light-emitting host polymer. As a result, LECs can emit light at voltages close to the band gap of the polymer, irrespective of the work function of the metal electrodes. However, conventional dynamic LECs require a finite charging time before they begin to emit light, making them unsuitable for applications requiring a rapid turn-on. Additionally, they are unsuitable for photovoltaic and current rectifying applications due to their symmetric current−voltage characteristics. These drawbacks have led to the development of fixed junction LECs in which the polarized ion distribution created under an applied voltage is subsequently fixed in place by creating a barrier to ion motion.[8−11] Such fixed junction devices, although requiring an initial poling step, improve turn-on times from seconds to milliseconds once the profiles have been established.[8] Due to their rectifying nature, fixed junctions can also exhibit a photovoltaic response.[9,11] Similar devices have also drastically improved the lifetimes of LECs with estimated lifetimes approaching 20 000 h at typical operating conditions.[3,11]

However, with the increasing interest in LECs and the use of new materials comes an increasing need to understand the fundamental processes underpinning LEC behavior in different systems. For instance, a variety of models have been put forward to explain LEC operation in various systems.[7,12,13] In an early paper, Pei et al. proposed a p-i-n junction model (Figure 1a and b), in which doping leads to the formation of n-type and p-type regions near the cathode and anode, respectively. In this model, an intrinsic region subsequently forms in the middle of the device and is responsible for both the emission and the

(1) Simon, D. T.; Stanislowski, D. B.; Carter, S. A. *Appl. Phys. Lett.* **2007**, *90*, 103508 (1−3).
(2) Shin, J. H.; Dzwilewski, A.; Iwasiewicz, A.; Xiao, S.; Fransson, A.; Ankah, G. N.; Edman, L. *Appl. Phys. Lett.* **2006**, *89*, 013509 (1−3).
(3) Zhang, Y. G.; Gao, J. *J. Appl. Phys.* **2006**, *100*, 084501 (1−8).
(4) Bernards, D. A.; Flores-Torres, S.; Abruna, H. D.; Malliaras, G. G. *Science* **2006**, *313*, 1416−1419.
(5) Parker, S. T.; Slinker, J. D.; Lowry, M. S.; Cox, M. P.; Bernhard, S.; Malliaras, G. G. *Chem. Mater.* **2005**, *17*, 3187−3190.
(6) Slinker, J. D.; Rivnay, J.; DeFranco, J. A.; Bernards, D. A.; Gorodetsky, A. A.; Parker, S. T.; Cox, M. P.; Rohl, R.; Malliaras, G. G.; Flores-Torres, S.; Abruna, H. D. *J. Appl. Phys.* **2006**, *99*, 074502 (1−3).
(7) Pei, Q. B.; Yu, G.; Zhang, C.; Yang, Y.; Heeger, A. J. *Science* **1995**, *269*, 1086−1088.
(8) Yu, G.; Cao, Y.; Andersson, M.; Gao, J.; Heeger, A. J. *Adv. Mater.* **1998**, *10*, 385−388.
(9) Leger, J. M.; Rodovsky, D. B.; Bartholomew, G. P. *Adv. Mater.* **2006**, *18*, 3130−3134.
(10) Cheng, C. H. W.; Lonergan, M. C. *J. Am. Chem. Soc.* **2004**, *126*, 10536−10537.
(11) Shao, Y.; Bazan, G. C.; Heeger, A. J. *Adv. Mater.* **2007**, *19*, 365−370.
(12) deMello, J. C.; Tessler, N.; Graham, S. C.; Friend, R. H. *Phys. Rev. B* **1998**, *57*, 12951−12963.
(13) Leger, J. M.; Carter, S. A.; Ruhstaller, B. *J. Appl. Phys.* **2005**, *98*, 124907 (1−7).

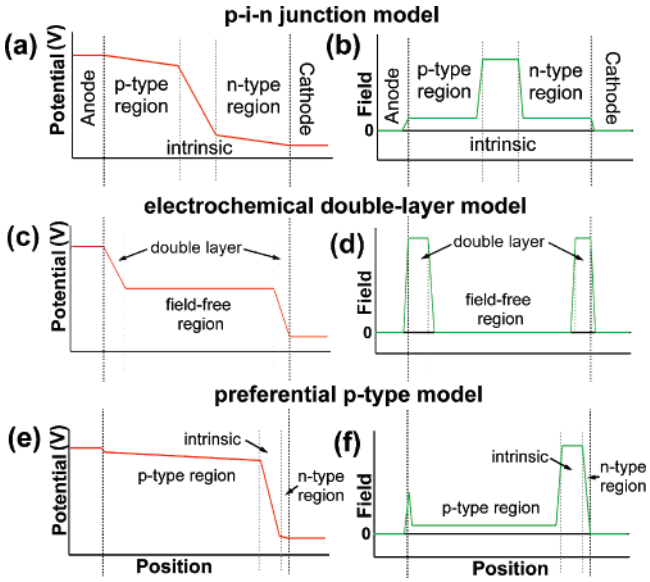

Figure 1. Idealized potential profiles and electric fields in light-emitting electrochemical cells as proposed by various authors for different materials systems: (a and b) p-i-n junction model after Pei, Heeger and co-workers, (c and d) electrochemical double layer model after de Mello, Friend and co-workers, (e and f) preferential p-type model as advocated by Leger, Carter and co-workers. For comparison with SKPM data the potential profiles are drawn with the cathode set to ground and the anode under positive bias (thus the diagrams differ from the classic band diagrams of doped semiconductor junctions).

majority of the potential drop.[7] This interpretation is consistent with calculations that assume the mobile ions are strongly associated in the polymer film.[14] In contrast, de Mello and co-workers proposed an electrochemical double layer model in which the potential is dropped over narrow charged double layers at each electrode (Figure 1c and d), rendering the bulk of the device free of an electric field. This picture suggests that carrier transport occurs primarily via diffusion through the bulk of the film.[12] Electroabsorption measurements performed by de Mello et al. provided evidence for the presence of a field-free region and, by inference, a large field drop at each electrode.[15] In contrast, however, electroabsorption experiments by Gao et al. indicated the presence of a large electric field within the bulk of the LEC.[16] Furthermore, optical beam induced current measurements on LECs frozen at 240 K while under bias provided evidence for the formation of a p-i-n junction in devices made with precursor-route PPV.[17]

In addition, more complicated models have been proposed to explain current transients in related systems. For example, studying a cationic conjugated ionomer, Lonergan and co-workers concluded that double layer charging predominates at low biases (below the polymer band gap) but that both n- and p-type doping occur at biases above the band gap.[18]

Recently, studying devices using soluble alkoxy-PPV derivatives as the emissive materials, with LiTf as the dopant salt, and PEO as a supporting matrix, several authors have discussed devices where p-type doping appears to dominate,[19−22] and Leger et al.[13] published a series of papers[13,23,24] supporting the preferential p-type model in which the bulk of the device undergoes reversible p-doping in the presence of negative counterions, the n-type region (if present) is confined to a small area near the cathode, and the bulk of the potential is dropped near the film/cathode interface (Figure 1e and f).[13,23,24] In their model, the high conductivity of the p-doped film is responsible for the small potential drop across the bulk of the device. Therefore, the bulk would appear to be free of any significant electric field, consistent with the measurements by de Mello et al.[15] Similar conclusions have been supported by other groups using fluorescence imaging of large (millimeter scale) planar devices.[2,21,25,26]

Although the models advocated by de Mello et al., Pei et al., and Leger et al. contain common elements related to ion motion, they do predict significant qualitative differences in the potential profiles and internal electric field distributions in operating LECs, as seen in Figure 1. These differences are perhaps unsurprising, given the differences in materials and experimental methods used between different groups. It is possible that different LECs may operate in each of the regimes (a), (c), or (e) depicted in Figure 1 (indeed, these models could also be viewed as different limiting cases along a common continuum). Also, these differences may influence the reduction and oxidation of different species within the device upon the application of voltages greater than the band gap of the polymer. For example, in the p-i-n model, the conjugated polymers act as both the reduced and oxidized species and light is emitted from the intrinsic region in the center of the device, whereas, in the preferential p-type model, the conjugated polymer may be oxidized with the corresponding negative charge building up at the surface of the cathode (or in a very small region of polymer near the cathode surface) until the large field at the cathode leads to electron injection, charge recombination, and electroluminescence which is subsequently observed very close to the cathode.

While studies based on fluorescence microscopy of planar LECs incorporating soluble alkoxy-PPVs appear to be converging to an interpretation consistent with the preferential p-type doping model (Figure 1e),[13,19−22,27−29] the optical methods generally used to study these systems are limited in their resolution and provide at best an indirect and qualitative probe of the doping profile that does not provide direct information about local potential or electric field values. While electroabsorption measurements can measure the average internal field,[15,30] the internal field is zero in both the electrochemical double layer and preferential p-type doping models.[3,13,15]

(14) Smith, D. L. *J. Appl. Phys.* **1997**, *81*, 2869−2880.
(15) deMello, J. C.; Halls, J. J. M.; Graham, S. C.; Tessler, N.; Friend, R. H. *Phys. Rev. Lett.* **2000**, *85*, 421−424.
(16) Gao, J.; Heeger, A. J.; Campbell, I. H.; Smith, D. L. *Phys. Rev. B* **1999**, *59*, R2482−R2485.
(17) Dick, D. J.; Heeger, A. J.; Yang, Y.; Pei, Q. B. *Adv. Mater.* **1996**, *8*, 985−987.
(18) Cheng, C. H. W.; Lin, F. D.; Lonergan, M. C. *J. Phys. Chem. B* **2005**, *109*, 10168−10178.
(19) Kaminorz, Y.; Smela, E.; Johansson, T.; Brehmer, L.; Andersson, M. R.; Inganas, O. *Synth. Met.* **2000**, *113*, 103−114.
(20) Gao, J.; Dane, J. *Appl. Phys. Lett.* **2003**, *83*, 3027−3029.
(21) Edman, L.; Summers, M. A.; Buratto, S. K.; Heeger, A. J. *Phys. Rev. B* **2004**, *70*, 115212 (1−7).
(22) Robinson, N. D.; Shin, J. H.; Berggren, M.; Edman, L. *Phys. Rev. B* **2006**, *74*, 155210 (1−5).
(23) Holt, A. L.; Leger, J. M.; Carter, S. A. *Appl. Phys. Lett.* **2005**, *86*, 123504 (1−3).
(24) Holt, A. L.; Leger, J. M.; Carter, S. A. *J. Chem. Phys.* **2005**, *123*, 044704 (1−7).
(25) Yu, G.; Pei, Q.; Heeger, A. J. *Appl. Phys. Lett.* **1997**, *70*, 934−936.
(26) Dane, J.; Tracy, C.; Gao, J. *Appl. Phys. Lett.* **2005**, *86*, 153509 (1−3).
(27) Hu, Y. F.; Gao, J. *Appl. Phys. Lett.* **2006**, *89*, 253514 (1−3).
(28) Shin, J. H.; Xiao, S.; Edman, L. *Adv. Funct. Mater.* **2006**, *16*, 949−956.
(29) Campbell, I. H.; Smith, D. L.; Neef, C. J.; Ferraris, J. P. *Appl. Phys. Lett.* **1998**, *72*, 2565−2567.

Thus, it is useful to apply additional tools to characterize LECs in order to address these questions. In addition to studying the operating mechanisms of classic LEC formulations, it is also important to compare the operating mechanisms of classic dynamic device formulations with those of newer formulations aimed at creating a fixed dopant distribution.[3,8,9,11,26] An examination of the temporal evolution of the potential profile in these devices may provide insight into the doping mechanisms and would be useful for guiding the synthesis of improved dopant pairs and host polymers. Additionally, such information could be relevant to the operation of LEC-like devices based on ionic transition metal complexes[4,5] which are being pursued for solid-state lighting applications.[6]

Ideally, one would like to make a direct measurement of the local potential profile across an LEC operating under bias at room temperature. Electrostatic force microscopy (EFM), Scanning Kelvin Probe Microscopy (SKPM), and related scanning probe based techniques are capable of directly imaging the local potential and charge distribution in thin film devices.[31,32] Indeed, scanning probe based methods have emerged as powerful tools for studying charge injection,[33,34] transport,[33,35] photocurrent generation,[36] and trapping[37,38] in organic electronic devices ranging from field-effect transistors[35] to solar cells.[36,39]

In this paper, we examine a variety of planar LECs[25] (gap width $\sim$15 μm) with Scanning Kelvin Probe Microscopy (SKPM)[40,41] and monitor the evolution of the potential profile between the two electrodes over time as the devices are biased in an inert atmosphere. As a reference point, we begin by examining a prototypical dynamic junction LEC fabricated with lithium trifluoromethanesulfonate (LiTf) salt, PEO, and the soluble alkoxy-PPV derivative MDMO-PPV and compare these results with the three models depicted in Figure 1. Subsequently, we study chemically fixed LECs based on cross-linked ion-pair monomers,[9] examine the evolution of the potential profile over time, and contrast the behavior of the chemically fixed LEC with that of the dynamic LEC.

2. Experimental Procedures

Materials. The materials used in this study include lithium trifluoromethanesulfonate (lithium triflate or LiTf), poly(ethylene oxide) (PEO), poly[2-methoxy-5-(3′,7′-dimethyl-octyloxy)-*p*-phenylenevinylene (MDMO-PPV), and the ion-pair monomer [2-(methacryloyloxy)-ethyl] trimethylammonium 2-(methacryloyloxy)ethanesulfonate (METMA/MES). LiTf and PEO were obtained from Sigma Aldrich and used as received. The light-emitting polymer MDMO-PPV was synthesized in-house using a Gilch polymerization route via dehydrohalogenation of appropriate precursors as outlined in the literature.[42]

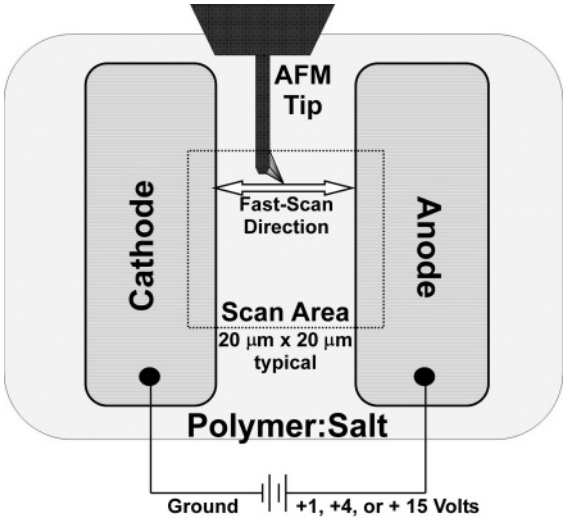

Figure 2. Schematic diagram of the experimental configuration. The polymer layer is spin-coated prior to electrode deposition. The AFM probe is raster-scanned across the interelectrode gap as noted in the figure. A typical scan area is shown in the image as the dashed box.

The average molecular weight was approximately 530 000, and the polydispersity index (PDI) was 1.03. The ion-pair monomer (IPM), METMA/MES, used in this study was synthesized by using commercially available starting materials by means of literature procedures.[9] (See Supporting Information for ^{1}H NMR results and the molecular structures of the molecules used.)

Device Fabrication. Planar LEC devices[7,8,16,26] were constructed in a single-layer architecture by spin-coating the polymer solution to a thickness of 200−500 nm (as determined by AFM measurements) onto glass substrates in a nitrogen glovebox (<0.4 ppm O_2). The solution composition was MDMO-PPV, PEO, and salt in an 8:1.5:X (X = 1.0 or 0.1 for 10 mol % and 1 mol %, respectively) ratio for the ion-pair monomer system and 8:3:1 for the LiTf system, both dissolved at approximately 1% by total weight in chlorobenzene. Assuming that all of the salt is active and the density of the polymer is $\sim$1 g/cm^3, this corresponds to an ionic charge density of $\sim 2 \times 10^{20}$/cm^3 for the 10 mol % ion-pair monomer samples, $\sim 2 \times 10^{19}$/cm^3 for the 1 mol % ion-pair monomer sample, and $\sim 5.5 \times 10^{20}$/cm^3 for the dynamic LiTf devices.

After spin-coating, the polymer films were annealed on a hot plate at 80 °C for 1 h in the drybox. The films were transferred to a thermal evaporator and dried under vacuum at 10^{-6} Torr overnight. The planar junctions were completed by depositing gold electrodes (50 nm thick) by thermal evaporation through a shadow mask at an average rate of 0.2 nm per s. The interelectrode gap was defined by pulling a spun-soft glass wool fiber taught over the mask (diameter range 23−30 μm), securing it onto the electrode mask, and subsequently fixing the substrates to the mask in conformal contact. After brief exposure (<1 min) to ambient conditions following the thermal evaporation step, the samples were transferred from the evaporator to a nitrogen glovebox. Top contacts were used to avoid screening effects due to the ions in the polymer. When bottom contacts were used, charge screening in the vertical direction complicated data analysis (see Supporting Information, Figure S1, for more details).

Scanning Probe Microscopy. SKPM measurements were performed using an Asylum Research MFP-3D atomic force microscope (AFM), a Stanford Research Systems model 830 lock-in amplifier, an Agilent Technologies 33120A function generator, and a custom-built adder amplifier. The AFM was also fitted with Asylum's fluid cell, enabling both imaging in inert (dry N_2) environments and the ability to load

(30) Brewer, P. J.; Lane, P. A.; de Mello, A. J.; Bradley, D. D. C.; deMello, J. C. *Adv. Funct. Mater.* **2004**, *14*, 562−570.
(31) Stern, J. E.; Terris, B. D.; Mamin, H. J.; Rugar, D. *Appl. Phys. Lett.* **1988**, *53*, 2717−2719.
(32) Martin, Y.; Abraham, D. W.; Wickramasinghe, H. K. *Appl. Phys. Lett.* **1988**, *52*, 1103−1105.
(33) Silveira, W. R.; Marohn, J. A. *Phys. Rev. Lett.* **2004**, *93*, 116104 (1−4).
(34) Burgi, L.; Richards, T. J.; Friend, R. H.; Sirringhaus, H. *J. Appl. Phys.* **2003**, *94*, 6129−6137.
(35) Burgi, L.; Richards, T.; Chiesa, M.; Friend, R. H.; Sirringhaus, H. *Synth. Met.* **2004**, *146*, 297−309.
(36) Coffey, D. C.; Ginger, D. S. *Nat. Mater.* **2006**, *5*, 735−740.
(37) Palermo, V.; Palma, M.; Samori, P. *Adv. Mater.* **2006**, *18*, 145−164.
(38) Muller, E. M.; Marohn, J. A. *Adv. Mater.* **2005**, *17*, 1410−1414.
(39) Palermo, V.; Ridolfi, G.; Talarico, A. M.; Favaretto, L.; Barbarella, G.; Camaioni, N.; Samori, P. **2007**, *17*, 472−478.
(40) Nonnenmacher, M.; Oboyle, M. P.; Wickramasinghe, H. K. *Appl. Phys. Lett.* **1991**, *58*, 2921−2923.
(41) Jacobs, H. O.; Knapp, H. F.; Muller, S.; Stemmer, A. *Ultramicroscopy* **1997**, *69*, 39−49.
(42) Becker, H.; Spreitzer, H.; Ibrom, K.; Kreuder, W. *Macromolecules* **1999**, *32*, 4925−4932.

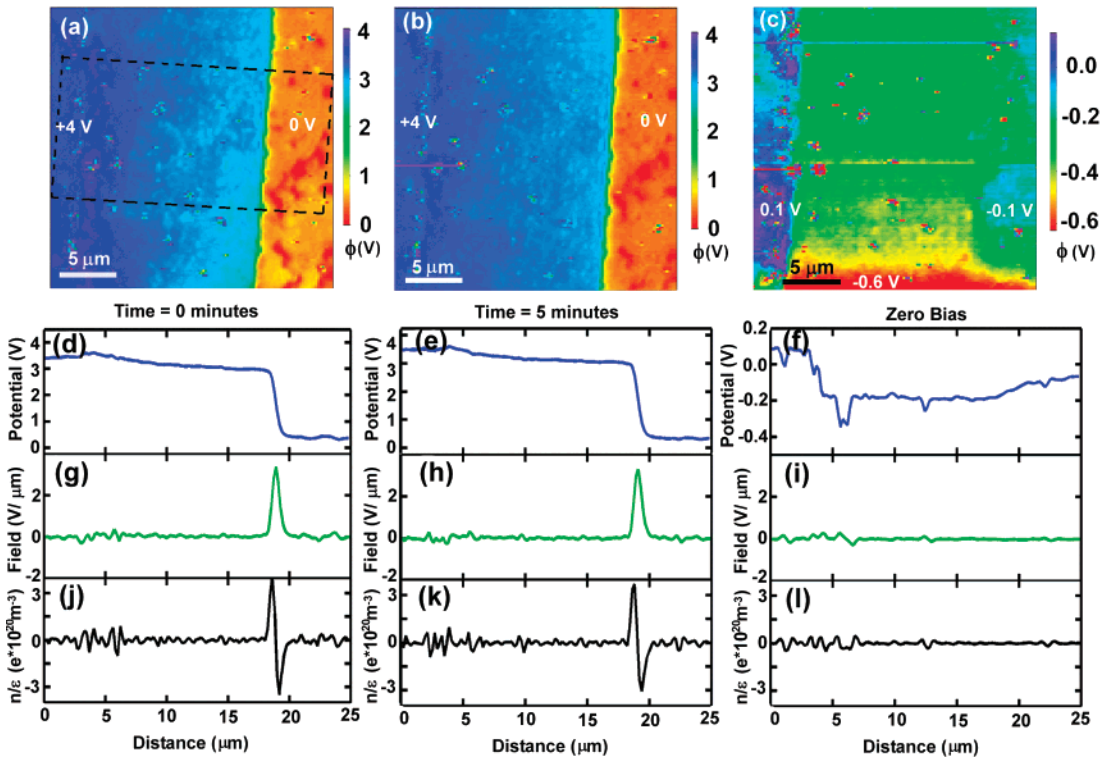

Figure 3. Scanning Kelvin Probe Microscopy (SKPM) images of LiTf-doped MDMO-PPV LECs under a 4 V bias. (a) Immediately after application of the bias, and (b) initiated after 16 min of driving at 4 V. There is little evolution of the profile over this time, and the majority of the potential drop is seen near the cathode. The corresponding line-averaged 1-D potential profiles can be seen in (d−f), gathered from the center regions of the device as shown in (a). (c) Image acquired after grounding both electrodes (note *z*-scale is ∼7× smaller). The image was acquired from the bottom to the top. The discharging of the device and the motion of the counterions can be seen in the bottom of the image. (g−i) Electric field profiles for (d−f) obtained by numerical differentiation of the voltage profiles. (j−l) Net elemental charge density profiles for (d−f) obtained by numerical differentiation of the field profiles.

samples into the flow-cell inside of a glovebox and then mount them in the AFM without ambient exposure. Cr/Pt coated silicon AFM probes (Tap300E) from BudgetSensors were chosen for these experiments with a ∼250 kHz resonance frequency (as measured) and a force constant of 40 N/m. All measurements were performed in noncontact mode so as to avoid tip wear and sample damage. During topography acquisition the AC bias applied during SKPM imaging was shut off. The electrode gap was located using an overhead digital video microscope for course alignment followed by SKPM imaging of the region with a small (∼1 Volt Direct Current, or VDC) bias applied across the planar device. Once the gap was located, scanning was performed in the direction perpendicular to the electrodes. A schematic representation of the experiment is displayed in Figure 2. Biases were always applied across the two electrodes at values of 0 VDC, +1 VDC, +4 VDC, or +15 VDC. The cantilever was oriented parallel to the long axis of the electrodes to minimize artifacts due to the capacitance between the cantilever beam and the electrodes.

The alternating current (AC) bias used for SKPM measurements was 2 V peak-to-peak, applied at 700 Hz (chosen to optimize signal/noise while remaining much lower than the cantilever drive frequency). A lift height of 40 nm was used for all SKPM measurements with a tip dwell time of 10 ms per pixel during SKPM image acquisition and a tip velocity of 10 μm/s during the topography scan. These values were chosen as an appropriate compromise among imaging stability, lateral resolution, and image acquisition time. A 4 VDC bias was applied across the electrodes during imaging, whereas 15 VDC was applied between scans to accelerate ion motion in the fixed ion-pair monomer devices. When aging the dynamic LiTf devices, a 4 VDC bias was used. The reported drive times are the time driven at 15 VDC, for the ion-pair monomer devices. The drive time accumulated during imaging at 4 V was not included in the cumulative time, except where noted (typical scan acquisition time was ∼12.5 min).

3. Results and Discussion

We first describe the results of SPKM imaging of conventional dynamic MDMO-PPV/PEO/LiTf planar devices. Figure 3 shows the surface potential of an MDMO-PPV/PEO/LiTf device immediately after applying a 4 V bias (Figure 3a), after holding at 4 V bias for 16 min (Figure 3b), and upon grounding the contacts (Figure 3c). The corresponding topography scan can be found in the Supporting Information (Figure S2). Figure 3d−f show the corresponding potential profiles averaged over 70 scan lines (corresponding to a 13.5 μm wide area shown in Figure 3a as 1D line traces). These line scans were acquired perpendicular to the electrode edge. The SKPM images in Figure 3a and b and the corresponding line traces in Figure 3d and e show a nearly constant potential across the device, with over 90% of the applied voltage dropping at the cathode, and almost no noticeable potential drop at the polymer/anode interface (see Supporting Information, "SKPM Images After Grounding Both Electrodes..." for additional details). These profiles are distinctly different from those taken on undoped polymer films (see Supporting Information, Figure S3).[43,44]

Of the three models for LEC operation discussed above, these data are by far the most consistent with the preferential p-type doping model[1,13,23,24] in which reversible p-doping facilitates formation of an ohmic contact at the anode and creates a low resistance channel across the device. The large potential drop observed at the cathode is consistent with either a very narrow,

(43) Ng, T. N.; Silveira, W. R.; Marohn, J. A. *Phys. Rev. Lett.* **2007**, *98*, 066101 (1−3).
(44) Puntambekar, K. P.; Pesavento, P. V.; Frisbie, C. D. *Appl. Phys. Lett.* **2003**, *83*, 5539−5541.

or no n-doped region in the MDMO-PPV/PEO/LiTf system. In this case electron injection is facilitated by the large electric field between the oxidized film and the accumulated electrons in the cathode. This is in good agreement with previous results based on fluorescence microscopy.[2,13,22] Furthermore, the plot of the local field vs position (Figure 3g−i, obtained by numerically differentiating the surface potential profile) shows that these data are also consistent with the electroabsorption measurements of de Mello et al.[15] which suggested that the bulk of the device was free of any significant electric field. Figure 3a and b show no changes outside the experimental noise between the first scan and the second scan taken 5 min later. This stability not only is indicative of the reproducibility of the potential profiles but also suggests that the counterion profile at this bias and concentration is established within 1 min of the application of the external bias (taking into account the finite time required to begin a scan after applying the bias). After tuning off the bias by grounding both electrodes, the device relaxes back to its equilibrium state within approximately 1 min (Figure 3c). The change in contrast from the bottom to the top of the image follows the device evolution in time, and we observe the tail end of the discharging process in the first few scan lines at the bottom of Figure 3c. As expected, very little uncompensated charge is stored within the device once the bias is removed (Figure 3l). The numerically derived charge profiles in Figure 3j−l (calculated by numerically differentiating the electric field profile and multiplying by ϵ_0/e) also reveal the small spatial extent of the charge accumulation regions near the junction. Although the exact width is difficult to determine due to the rough edge of the evaporated metal, the maximum fwhm of the region over which the potential is dropped, as determined from the averaged field profile (Figure 3h), is ∼0.85 μm. The actual region over which the potential is dropped is likely to be narrower, as this value is widened by a combination of the roughness of the electrode edge, the scan resolution of the acquired images, and tip convolution effects.[45,46]

We also used SKPM to examine the potential profile after the bias was reversed. Figure 4a shows the SKPM scan initiated immediately after the bias was switched from +4 V to −4V. The scan direction is from bottom to top, and a slight evolution of the potential profile is again observed over the course of the first minute or two after the bias is changed. However, due to the high ion concentration and high ion mobility in this blend, the redistribution of the potential profile is complete after less than 2 min. The corresponding line trace in Figure 4b appears as a mirror image to that in Figure 3a, underscoring the reversibility of the LEC device structure and symmetry of the contacts. This profile is also stable in time, as already discussed for the profiles shown in Figure 3.

While our results may appear at odds with the reports by Heeger and co-workers of the observation of a symmetric p-i-n junction in LECs formed with precursor-route PPV, we note that there our several differences between the experiments. In addition to being conducted under bias at room temperature (as opposed to short circuit after prebias at 240 K in Dick et al.[17]), our measurements are performed on devices using soluble alkoxy-PPV derivatives. Our direct observation of a large

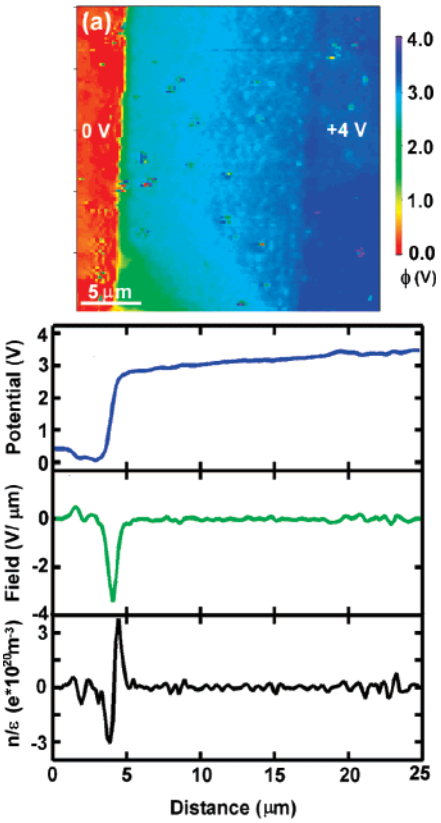

Figure 4. (a) SKPM image gathered immediately following a reverse in polarity (from +4 V to −4 V). The scan was initiated at the bottom of the image. Some motion of the counterions is observed near the bottom of the image, but the potential profile stabilized after ∼2 min. (b) Corresponding potential profile, (c) numerically derived electric field distribution, and (d) net elemental charge density.

potential drop near the cathode is thus consistent with the majority of the optical studies on LECs made from soluble PPV derivatives which report that the emission zone is typically localized very near the cathode.[7,13,20−22,24,29] These results suggest either that in many commonly studied devices there is a large barrier to electron injection (reduction overpotential) even in the presence of the compensating counterions and accumulated electrons in the cathode or alternatively that the reduced state is unstable in the solid-state electrochemical matrix as prepared. The reasons reversible n-doping may be observed in some systems but not others remains an open question, but the difficulty in achieving n-doping is consistent with the difficulty in achieving reversible reduction waves in solution electrochemistry experiments[23,24] and with the observation that the use of Li cations can lead to preferential p-doping in solid-state devices due to issues of counterion mobility.[27] These results reinforce the need to perform independent characterization before interpreting the device behavior of a given LEC structure in the context of one of the models depicted in Figure 1.

Having established a reference point for device operation by using SKPM to directly image the potential profiles in dynamic LECs based on conventional MDMO-PPV/PEO/LiTf blends, we now turn our attention to the more complicated case of fixed-junction LECs prepared from MDMO-PPV blends where the LiTf ions are replaced with the ion-pair monomer METMA/MES. Previous work on this system suggests that during the initial poling step METMA/MES polymerizes due to radical initiation upon charge carrier injection.[9] This forms an immobile

(45) Liscio, A.; Palermo, V.; Gentilini, D.; Nolde, F.; Mullen, K.; Samori, P. *Adv. Funct. Mater.* **2006**, *16*, 1407−1416.
(46) Zerweck, U.; Loppacher, C.; Otto, T.; Grafstrom, S.; Eng, L. M. *Phys. Rev. B* **2005**, *71*, 125424 (1−3).

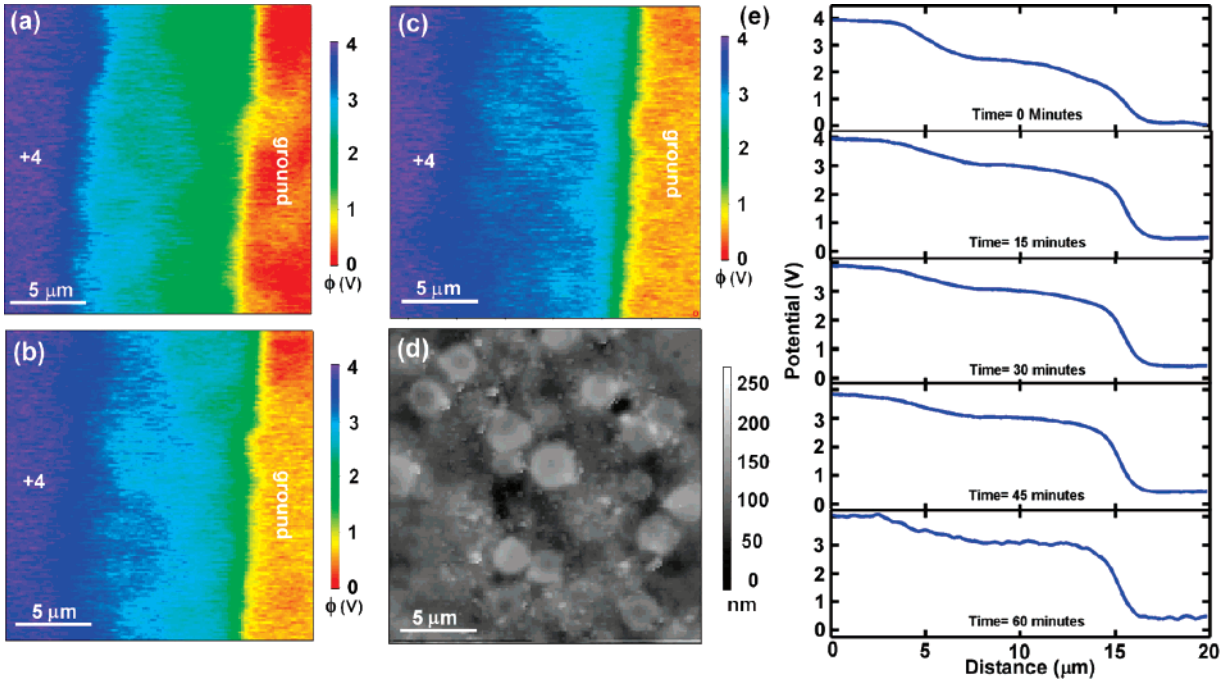

Figure 5. (a−c) SPKM images of a 10 mol % METMA/MES-doped LEC after (a) 0 min, (b), 15 min, and (c) 60 min. (d) Corresponding topography image. (e) Corresponding line traces of the potential averaged over 70 lines.

species that "locks in" the counterion distribution even upon the removal of the external bias, thus creating a permanently polarized LEC device.[9] Although device measurements provide evidence for the frozen nature of the junction,[9] there have been no studies of the resulting potential profile or its evolution during the poling process.

Figure 5 shows the SKPM imaging of devices with an ion-pair monomer concentration of ∼10 mol %, similar to those initially reported by Leger et al.[9] The SKPM profiles of the devices with the ion-pair monomers are less uniform than in the case for the dynamic LiTf-based LECs. We attribute this to the large-scale phase separation observed between the ion-pair monomer dopants and the polymer host that is observed in the AFM topography image (Figure 5d). Clearly, this phase-separation could have an impact on the performance of an operating LEC (see Supporting Information, Figure S4 for potential profiles of individual line scans).[47] However, we leave the effects of phase separation for a future study and focus on the average potential profiles here. At short times (less than 5 min) the potential drop is distributed across the anode/film interface (35%), the cathode/film interface (35%), and the bulk of the film (30%) (Figure 5a). The potential profile continues to evolve over 60 min until the majority (65%) of the potential is dropped very close to the cathode (Figure 5c) while a small portion of the applied bias is dropped at the anode. Figure 6 shows the corresponding field and charge density profiles that accompany the SKPM images in Figure 5. Immediately after applying the bias (Figure 6a) the largest fields are at the contacts, indicative of injection-limited currents. Over the next 15−45 min (Figure 6b−e) the field and uncompensated charge at the anode decrease as the oxidative doping process proceeds. After 60 min, the final potential and field profiles resemble those obtained with shorter equilibration times (<1 min) in the dynamic LEC (Figure 3a) and are thus qualitatively consistent with a predominately p-doped device and a large field at the cathode/film interface. However, in the fixed LECs the potential drop at the anode/polymer contact and the potential drop through the bulk of the film are both larger than those in the dynamic LECs. We attribute both the substantially slower response time and the residual contact resistance at the anode/polymer film to the lower ionic mobility of the METMA/MES pair in the MDMO-PPV/PEO matrix relative to that of the LiTf. The low ionic mobility responsible for the slow response could lead to premature carrier-induced radical polymerization of the ion pair monomer on a time scale comparable to the equilibration time of the ions. These factors would explain the incomplete compensation at the anode in the planar devices studied here (although we cannot exclude the possibility that the poor solubility of the METMA/MES in the MDMO-PPV/PEO matrix also plays a role, an effect which would also be consistent with the larger field drop and apparent lower conductivity of the METMA/MES-doped film).

Significantly, the slow ion motion allows us to resolve the evolution of the potential profile in time. Based on fluorescence microscopy on dynamic LECs,[2,21,26] it has been suggested that p-doping in dynamic LECs proceeds via the propagation of a steplike "front" of a highly doped polymer beginning at the anode and moving across the device until the p-doped region reaches the cathode. Interestingly, we do not see such a progression in these micron-scale devices prepared with the ion-pair monomers, as this would be seen as a propagation of a steplike potential drop across the device over time. Instead, we observe a slow increase in the intermediate potential in the device accompanied by an increase in the width of the anode side potential drop as seen in Figure 5a−c and Figure 6a−e. These results might suggest that the profile evolution is dominated by the slow dissociation and motion of counterion pairs under the applied bias. At lower dopant concentrations (1 mol %, see Supporting Information, Figure S5), the phase

(47) The rough topography may also degrade the SKPM image quality.

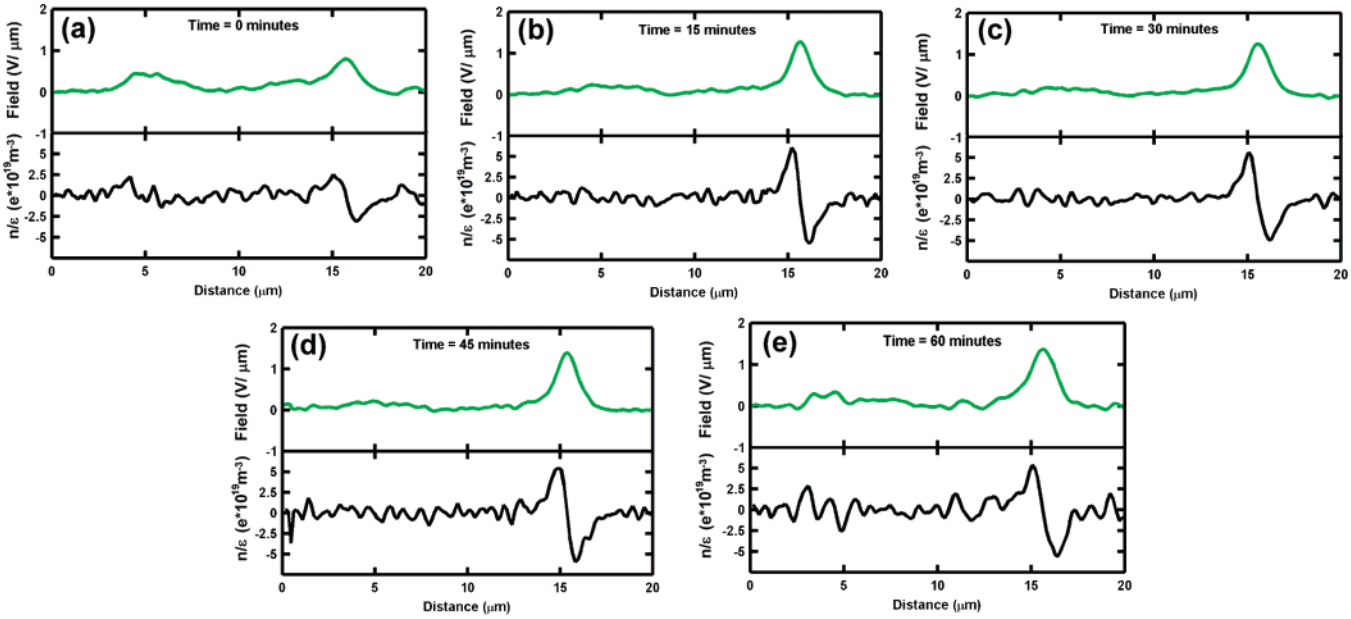

Figure 6. Field profiles and net elemental charge density profiles from the potential profiles shown in Figure 5e. A three-point moving average was used on the field profiles prior to differentiation.

separation observed in Figure 5d is greatly diminished, the potential profile evolves more slowly, and there remains a larger drop in the potential at the anode/film interface at long times. After grounding both electrodes, evidence for frozen counterion distributions can be also observed in the SKPM images for both the 10 mol % and 1 mol % samples (see Supporting Information, Figure S6).

4. Conclusions

We have used SKPM to study the potential profiles and electric field distributions in both dynamic LECs doped with LiTf and fixed LECs doped with the ion-pair monomer METMA/MES. We have shown that in dynamic LiTf-doped LECs made using MDMO-PPV the potential profile measured by SKPM is consistent with the preferential p-type doping model,[13] with a low-resistance contact at the polymer/anode interface, very little electric field across the bulk of the polymer film, and ~90% of the potential being dropped at the polymer/cathode interface. We find that this potential distribution is reached in less than 1 min. This potential profile, based on direct local potentiometry, is in excellent agreement with the indirect measurements of the doping profiles of similar alkoxy-PPV-based LEC devices that have been inferred from fluorescence quenching in optical microscopy.[2,21,25,26] The reason this common materials combination appears to operate in the preferential p-type doping limit advocated by Leger et al., as opposed to the ideal symmetric p-i-n junction limit reported in some devices studied by Heeger and co-workers, remains an open question; however, we speculate that it could be related to differences between precursor-route PPV and soluble derivatives of PPV,[21] the testing conditions (room T under bias vs low T under short circuit),[15] or could also be linked to counterion mobility in the films,[27] or even trapping. Under these conditions charge conservation is maintained through the accumulation of electrons in the cathode and/or the formation of a small n-doped region near the surface of the cathode. However, the width of any n-doped region is constrained by the imaging to be less than 1.0 μm.

When the external bias is removed, the LiTf-doped LECs discharge in a matter of minutes. In contrast, fixed junction LECs doped with the ion-pair monomer METMA/MES show qualitatively different behavior. When first poled, we find that the applied potential is distributed between the anode/polymer interface, the polymer bulk and the cathode/polymer interface at short times (minutes) due to the slow ion motion. Ultimately, after poling for ~45−60 min, these fixed junction LECs evolve toward the same limit as the dynamic LECs, but with larger residual potential drops at the polymer/anode interface and across the polymer bulk. The time evolution of the potential in fixed LECs does not appear consistent with the movement of a uniform front of a heavily doped polymer propagating from anode to cathode. We attribute the slower charging response of the ion pair monomer LECs versus the LiTf doped LECs to the lower ionic mobility of the METMA/MES pair. Not only do these results demonstrate that scanning probe microscopy can be a valuable tool in the study and optimization of LECs, but furthermore, this work suggests that the chemically fixed LECs studied herein might be improved by increasing the ion mobility, by obtaining better control of the radical reaction that leads to immobilization of the ion-pair monomers, and by achieving better balance between n-type and p-type doping in this system. Synthetic efforts toward these goals are already underway, but our results specifically highlight these needs. Future studies will need to consider the effects of micro- and nanoscale dopant phase separation on device performance.

Acknowledgment. L.S.C.P., D.C.C., and D.S.G. acknowledge the support of the NSF (DMR 0449422 and 0120967), and D.S.G. thanks the Camille Dreyfus Teacher-Scholar Awards Program for support. D.S.G. is a Cottrell Scholar of Research Corporation and an Alfred P. Sloan Foundation Research Fellow. L.S.C.P. is an NSF Discovery Corps Fellow (CHE 0725139). D.B.R. and G.P.B. acknowledge the support of the NSF-STC (DMR 0120967). We thank Dr. Janelle Leger for discussions throughout this work.

Note Added in Proof: While this manuscript was under review, Marohn, Malliaras, and coworkers published an electric force microscopy study of light-emitting electrochemical cells containing a $[Ru(bpy)_3]^{2+}(PF_6^-)_2$ compound. They concluded that the majority of the potential drop in that class of devices also occurs at the cathode.[48]

Supporting Information Available: The ^1H NMR data for the METMA/MES monomers; topography image of the device shown in Figures 3 and 4; SKPM images from bottom contact devices with explanatory schematics; SKPM results from undoped MDMO-PPV devices; individual line potential profiles for a 10 mol % ion-pair monomer system; SKPM images from a 1 mol % ion-pair monomer system with corresponding potential profiles; and SKPM images acquired after driving the ion-pair monomer systems for 1 h and subsequently grounding both electrodes (including a more detailed image of the electrodes is available in the Supporting Information). This material is available free of charge via the Internet at http://pubs.acs.org.

JA074760M

(48) Slinker, J. D.; DeFranco, J. A.; Jaquith, M. J.; Silveira, W. R.; Zhong, Y.-W.; Moran-Mirabal, J. M.; Craighead, H. G.; Abruna, H. D.; Marohn, J. A.; Malliaras, G. G. *Nat. Mater*. **2007**, *6*, 894−899.